Available online at www.sciencedirect.com
ScienceDirect
Journal of Power Sources 164 (2007) 890–895
JOURNAL OF POWER SOURCES
www.elsevier.com/locate/jpowsour

Short communication

Electrochemical investigation of the anodic corrosion of Pb–Ca–Sn–Li grid alloy in H_2SO_4 solution

Reza Karimi Shervedani *, Asghar Zeini Isfahani, Rasool Khodavisy, Abdolhamid Hatefi-Mehrjardi

Department of Chemistry, University of Isfahan, Isfahan 81746-73441, Islamic Republic of Iran

Received 18 March 2006; received in revised form 11 October 2006; accepted 24 October 2006

Abstract

The steady-state and anodic corrosion of Pb–0.17 wt.% Ca–0.88 wt.% Sn, and Pb–0.17 wt.% Ca–0.88 wt.% Sn–0.06 wt.% Li alloys in 4.5 M H_2SO_4 at 25 °C were studied using cyclic voltammetry, linear sweep voltammetry, and electrochemical impedance spectroscopy. The experimental results show that the lithium added to Pb–Ca–Sn alloy increases corrosion resistance in equilibrium potential and inhibits the growth of the anodic corrosion layer.

Keywords: Pb–Ca–Sn–Li alloy; Lead-acid battery; Lithium; Anodic Pb^{2+} film; Electrochemical impedance spectroscopy (EIS)

1. Introduction

The main challenge for lead-acid batteries to become effective power sources for vehicle is the need to increase specific energy and to extend deep cycle life. To this end, efforts have been made to reduce significantly the dead weight from non-energy producing components (i.e., grids, connectors, terminals, etc.) and to increase both the electrode-material utilization and battery cycle life. These objectives are approached through the use of thin positive and negative plates, which are produced, from highly corrosion-resistant alloys [1]. The positive electrode has a strong effect on battery performance, and irreversibly degrades by a series of corrosion reaction. This early failure is attributed to the development of an insulating barrier layer at the interface between the positive grid and active material [2,3]. The use of pure lead gives rise to a strong oxide passive layer formation at the grid/active-material interface [4,5]. This oxide layer is highly stable in the acidic environment present in lead-acid batteries. The insulating passive film reduces the anode dissolution thereby increasing the active life of the battery [6]. However, this also has an undesirable effect of increasing the impedance of the anode after storage for a certain period of time. The increased resistance reduces the reversibility and charging efficiency during subsequent cycles [7,8].

Several studies have looked at the nature of the passive film formed on the anode. The composition of the passive layer is a mixture of $PbSO_4/PbO_x$ ($1 < x < 2$) [9–11]. The lead alloys, generally used as positive grids, are Pb–Sb and Pb–Ca alloys [10,11]. It was reported that Pb–Sb alloy is corroded and the complex antimony ions are formed as oxidized species [12]. These ions slowly migrate through the positive active material and the electrolyte and, then, antimony deposits on the negative electrode, lowering the overpotential of hydrogen evolution and give rise to increase self-discharge, excessive water loss or increased maintenance and decreased charge efficiency [10]. Hertz et al. [13] and Rocca and co-workers [14] reported that calcium is only added to enhance the mechanical properties of the lead alloys and has no influence on their electrochemical behavior. But Pavlov et al. [15] and Caillerie and Albert [16] reported that calcium increases the overpotential of hydrogen evolution on lead alloy and results in improving the performance of maintenance-free for the batteries. However, the lead–calcium alloy has poor strength and casting performance. Especially, a high-impedance passivation layer formed on Pb–Ca alloy during anodization can give rise to the detrimental influences on the deep charge/discharge cycle performance of the batteries

* Corresponding author. Tel.: +98 311 7932715; fax: +98 311 7932700.
E-mail address: rkarimi@sci.ui.ac.ir (R.K. Shervedani).

0378-7753/$ – see front matter © 2006 Elsevier B.V. All rights reserved.
doi:10.1016/j.jpowsour.2006.10.105

[15,16]. One of the most effective methods is to add tin into the lead alloy to improve the conductivity of the anodic film [14]. It has been reported that tin plays a complex role in the passivation phenomenon of lead tin alloys in sulfuric acid. At high tin level (1.5 wt.% < Sn) the PbO growth progressively decreases, and then electronic conductivity of the oxide layer is increased. At this tin level, the alloy is two-phased, which promotes the formation of a very thin and highly conducting oxide layer [14]. Alloying tin appears to favor the formation of an intermediate oxide, PbO_x, which is less resistive than PbO [17]. However, the deep charge/discharge cycle performance of Pb–Ca–Sn is still not satisfactory. Moreover, tin dissolves in the electrolyte from the alloy and forms Sn^{2+}. The reaction of Sn^{2+}/Sn^{4+} redox couple with the active materials of the positive and negative electrodes may increase the self-discharge of the batteries [10,18].

Metal elements such as strontium, cerium, and lithium, whose electrode potentials are close or more negative than that of calcium, may be added into lead or lead alloys to improve the crystal grain structure of the alloys and not obviously to decrease the hydrogen overpotential. The effect of cerium on the corrosion of Pb–Ca–Sn has been studied previously [10]. Although lithium has also an electrode potential close to that of calcium, to our knowledge, lithium has never been tested as an additive for improvement the performance of positive grid materials in lead-acid batteries. Specially, there is no quantitative electrochemical information on the effect of lithium incorporation in Pb–Ca–Sn alloy. In the present work, the anodic behavior of Pb–Ca–Sn–Li alloy was studied in sulfuric acid solution by electrochemical methods to clarify the possibility of its preparation as a positive grid material for lead-acid batteries. For this purpose, initially corrosion of alloy in equilibrium potential and finally in the battery deep discharge potential is considered.

2. Experimental

A lead–0.17 wt.% calcium–0.88 wt.% tin alloy and a lead–0.17 wt.% calcium–0.88 wt.% tin–0.06 wt.% lithium alloy were used as working electrodes. The alloys were prepared by melting the mixture of metals in furnace under argon gas atmosphere, and their composition was determined by atomic absorption spectroscopy (AAS). The electrolyte was 4.5 M H_2SO_4 solution prepared from H_2SO_4 and double-distilled water. All reagents were of analytical grade and obtained from Merck® or other commercial resources.

For electrochemical measurements, a three-electrode conventional glass cell was used. A sample was prepared from each alloy and welded to a copper wire to be used as working electrode for electrochemical measurements. The sides and other parts of the working electrode were covered with an epoxy resin (special polyester) to avoid any contact with electrolyte solution, except electrode surface exposing a 0.5 cm × 0.5 cm surface area of the alloy. A flat working-electrode surface was obtained by mechanical polishing with emery paper of successively decreasing grain size down to 10 μm. Then, the working electrode was washed with double-distilled water before immersing in electrolyte solution. The electrolyte was a 4.5 M H_2SO_4 solution. Before each experiment, a cathodic potential of −1.2 V was applied for 20 min in order to reduce any oxide formed during pretreatment. A $Hg/Hg_2SO_4/H_2SO_4$ (4.5 M) electrode served as the reference ($E^{0'} = 0.630$ V at 25 °C). All potentials reported here are referenced to this electrode. A platinum plate (Pt 99.99%) was used as counter electrode. Electrochemical impedance spectroscopy (EIS), open circuit potential (OCP), cyclic voltammetry (CV), and linear sweep voltammetry (LSV) measurements were performed using EG&G P/G 273A/92 coupled to a frequency response analyzer EG&G FRA 1052 and controlled by a personal computer through GPIB-IEEE NI-488-II card. For the EIS measurements, a sine wave with 5 mV amplitude was applied at each dc potential, and a range of frequencies from 100 kHz to 0.1 Hz was scanned in logarithmic scale with 10 points/decade. The EIS data were approximated using complex nonlinear least square (CNLS) method and appropriate electronic equivalent circuit models built in ZView®2.3 software (Scribner Associates, Inc.), and the model parameters such as interfacial charge transfer resistance (R_{ct}) and double layer capacitance were estimated [19,20].

3. Results and discussion

3.1. Synthesis of working electrodes

Because of a large difference between the melting points of Li and Ca, the Pb–Ca–Sn–Li alloy was prepared in a three-step method as: (i) a sample of Pb–Ca alloy was prepared by mixing pure pellets of corresponding metals (typically 9.5 g of Pb with 0.5 g of Ca) and melted under argon gas atmosphere at 850 °C for 10 min in an electrical furnace, cooled down to 500 °C, kept under these conditions for 4 h to form homogeneous Pb–Ca alloy, then cooled to room temperature, and used for further works; (ii) a sample of Pb–Li alloy was also prepared by mixing pure pellets of corresponding metals (typically 9.7 g of Pb with 3 g of Li) and melted under argon gas atmosphere at 300 °C for 10 min, then cooled down to 120 °C, kept under these conditions for 4 h to form homogeneous Pb–Li alloy, then cooled to room temperature, and kept for further works; and (iii) appropriate percent of the Pb–Ca and Pb–Li alloys were mixed with Sn pellets, heated at 600 °C for 10 min, cooled down to 300 °C, kept under these conditions for 4 h to form homogeneous Pb–Ca–Sn–Li alloy, then cooled to room temperature, and used for preparation of working electrodes. The Pb–Ca–Sn was prepared by mixing appropriate percent of the Pb–Ca alloy, with Pb and Sn pure pellets, and heated as step (iii). The Pb–Ca–Sn and Pb–Ca–Sn–Li prepared by mixing different percent of Pb–Ca and Pb–Li with Sn, were analyzed in the same way by AAS.

Bulk homogeneity of the prepared alloys was determined by dissolution of local samples in acidic solution and analysis by AAS. The local samples were cut from bulk as well as surface of the prepared alloys. We expected 5 and 3% of Ca and Li in Pb–Ca and Pb–Li binary alloys, but we found 4.49 and 1.95%, in the bulks, and higher concentration of Ca and Li in the form of oxides and impurities on the sides and surfaces. Finally, lead–0.17 wt.% calcium–0.88 wt.% tin and lead–0.17 wt.% calcium–0.88 wt.% tin–0.06 wt.% lithium alloys were selected and used as working electrodes for electrochemical studies. The percent of Pb, Ca,

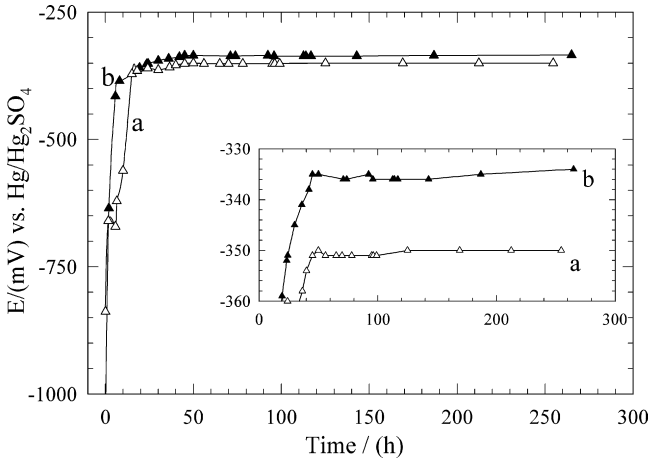

Fig. 1. Open circuit potential vs. time obtained on (a) Pb–Ca–Sn and (b) Pb–Ca–Sn–Li electrodes in 4.5 M H_2SO_4 at 25 °C.

and Sn in these alloys was more near to that of recently prepared Pb–Ca–Sn grids [1,10,14].

3.2. Electrochemical studies

3.2.1. Open circuit potential decay

The open circuit potential behavior of Pb–Ca–Sn and Pb–Ca–Sn–Li alloys is illustrated in Fig. 1. In both cases, the initial OCP potentials were almost −0.900 V but, they increased as functions of time and reached to different steady values (corrosion potential, E_{corr}) after 45 h. These values are −0.335 and −0.351 V for Pb–Ca–Sn and Pb–Ca–Sn–Li alloys, respectively, which are different by almost 0.016 V. Despite this small shift, the steady-state polarization behavior showed that the corrosion behavior of Pb–Ca–Sn is improved by addition of Li to this alloy.

3.2.2. Steady-state polarization

The steady-state polarization curves (Tafel plots), obtained on Pb–Ca–Sn and Pb–Ca–Sn–Li electrodes after 48 h immersion in 4.5 M H_2SO_4 solution at 25 °C are presented in Fig. 2. The corrosion current density (i_{corr}) associated with polarization measurement for the two samples were simultaneously determined in the potential range ±60 mV from E_{corr} using $i_{corr} = (\beta_a\beta_c)/[2.303R_p(\beta_a + \beta_c)]$ in which $\beta_a\beta_c$ are anodic and cathodic Tafel slopes, $R_p = \eta/i = RT/nFi_0$, η is overvoltage, i_0 exchange current density, and R, T, and n have their usual meanings [21]. The results obtained showed that the values of i_{corr} are 11.32×10^{-5} and 4.24×10^{-5} A cm^{-2} for Pb–Ca–Sn and Pb–Ca–Sn–Li alloys, respectively. The i_{corr} and its corresponding potential, E_{corr}, could also be directly estimated from interpolation of the linear parts of Tafel curves at higher η. The corrosion rates estimated from i_{corr} are of 134.2 and 50.3 mpy for Pb–Ca–Sn and Pb–Ca–Sn–Li alloys, respectively. These results show a large decrease in the corrosion rate of Pb–Ca–Sn by addition of Li to this alloy.

3.2.3. Cyclic polarization (CP)

The cyclic polarization curves obtained on Pb–Ca–Sn and Pb–Ca–Sn–Li alloys at 1 mV s^{-1} scan rate, between −0.430 and +0.640 V, after 48 h immersion in 4.5 M H_2SO_4 solution at 25 °C are presented in Fig. 3. One should consider that experiments are extended to more anodic potential regions in comparison to Fig. 2. Two passivation regions in anodic branches which are due to formation of two different kinds of lead compounds (non-stoichiometric sulfate and oxy-sulfate) and a small negative hysteresis effect in both plots are observed. The hysteresis effect implies that no pitting corrosion exists in these alloys. Moreover, the currents are lower for Pb–Ca–Sn–Li alloy. These behaviors also show that addition of Li to Pb–Ca–Sn has increased the stability of this alloy against anodic corrosion.

3.2.4. Electrochemical impedance spectroscopy

The EIS is a powerful, nondestructive, and informative technique, which is usually used for characterization and study of corrosion phenomena [22], fuel cells and batteries [23], coatings and conductive polymers [24], adsorption behavior of thin films [25–27], and electron transfer kinetics [28]. Recently, the EIS has been used in studies of lead-acid batteries for in situ characterization of anodic films formed on antimony and lead–antimony alloys in lead-acid batteries [29,30]. This method was used to investigate the anodic charge transfer resistance of Pb–Ca–Sn–Li new grid prepared in this work.

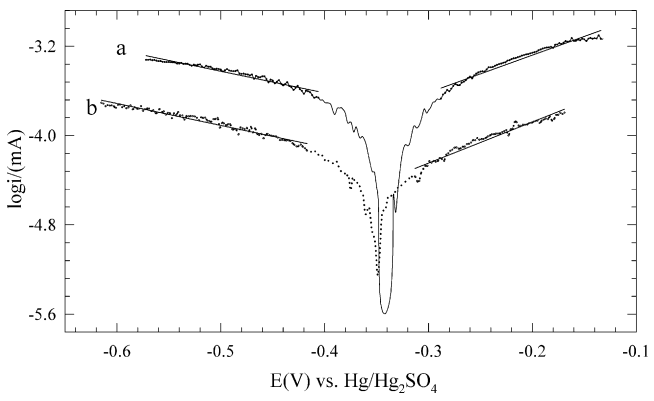

Fig. 2. Steady-state polarization curves (Tafel plots) obtained on (a) Pb–Ca–Sn and (b) Pb–Ca–Sn–Li electrodes after 48 h immersion in 4.5 M H_2SO_4 at 25 °C and then scanning the electrode potential with 1 mV s^{-1} scan rate.

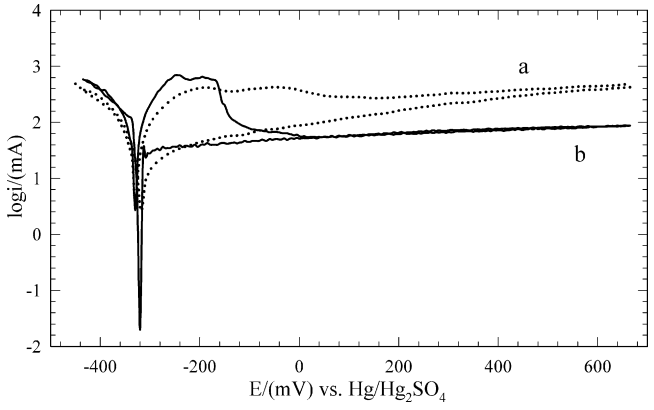

Fig. 3. Cyclic polarization curve obtained on (a) Pb–Ca–Sn and (b) Pb–Ca–Sn–Li electrodes after 48 h immersion in 4.5 M H_2SO_4 at 25 °C and then scanning the electrodes potential between −0.450 and +0.660 V with 1 mV s^{-1} scan rate.

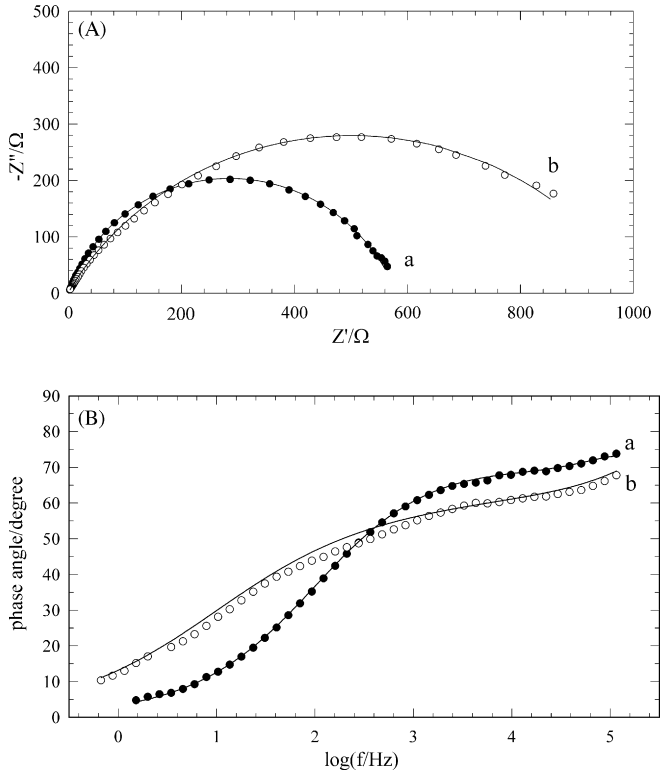

Fig. 4. (A) Complex plane and (B) phase angle plots obtained on (a) Pb–Ca–Sn and (b) Pb–Ca–Sn–Li electrodes in 4.5 M H_2SO_4 at OCP and 25 °C. Dots are experimental data and lines are fitted results obtained using CNLS method and ZView2.3.

A sample of the complex plane and Bode plots obtained on Pb–Ca–Sn and Pb–Ca–Sn–Li alloys after 48 h immersion in 4.5 M H_2SO_4 solution at OCP and 25 °C is presented in Fig. 4A and B. The EIS data reveal that each impedance diagram consists almost of two semicircles (capacitive loops). The electrode impedance in this case was determined by the metal/oxide interface, the oxide film, and the oxide/solution interface.

The data were approximated using different electronic equivalent circuits built in ZView2.3® software, and finally the best fit (the smallest χ^2) [31] was observed based on equivalent circuit Fig. 5 in which R_1 denotes solution resistance, R_2 and C indicate oxide layer resistance and capacitance, R_3 and CPE [20] represent charge transfer resistance and constant phase element of the oxide/solution interface, and parameter n explains deviation of the semicircle from its ideal form (i.e., time constant dispersion), and was attributed to inhomogeneities of the electrode surface. The values obtained at OCP for corrosion charge transfer resistance, R_3, were 558 and 920 Ω for Pb–Ca–Sn and Pb–Ca–Sn–Li, respectively. The same tendency was observed up to 1 V anodic overpotentials; however, the difference was larger for higher overpotentials (Fig. 6). It means that anodic films formed on Pb–Ca–Sn–Li at higher overpotentials resist against corrosion better than those formed on Pb–Ca–Sn alloy in these conditions. Therefore, the EIS results also show that the corrosion resistance of Pb–Ca–Sn is substantially improved by the presence of Li in this alloy. These data are in good agreements with those obtained from Tafel plots and cyclic polarization curves, Figs. 2 and 3.

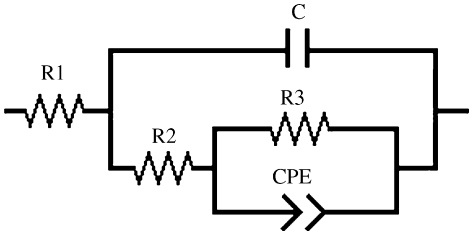

Fig. 5. Equivalent circuit diagram purposed for impedance behavior of the Pb–Ca–Sn and Pb–Ca–Sn–Li electrodes in 4.5 M H_2SO_4 at OCP and 25 °C.

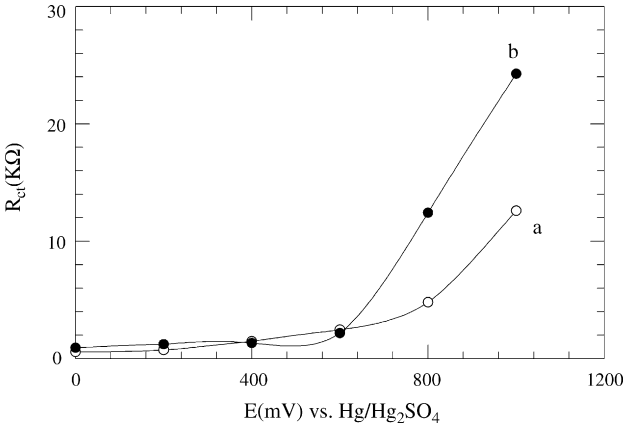

Fig. 6. Variation of the charge transfer resistance as a function of potential obtained on (a) Pb–Ca–Sn and (b) Pb–Ca–Sn–Li electrodes (see Figs. 4 and 5).

3.2.5. Linear sweep voltammetry

The LSV experiments were also performed to investigate the electrochemical stability and corrosion resistance of the Pb–Ca–Sn–Li grids. Therefore, the electrodes were anodized at +0.900 V in 4.5 M H_2SO_4 solution at 25 °C for 5, 10, 20, 30, 60, and 120 min, and then the electrode potential was swept to −1.2 V with 1 mV s^{-1} scan rate to reduce the oxides formed. The potential +0.900 V was chosen for the anodic film growth, because it is close to the positive grid potential after deep discharge in the batteries. A typical voltammogram obtained for reduction of the anodic films formed on Pb–Ca–Sn and Pb–Ca–Sn–Li alloys after 30 min anodization at +0.900 V is presented in Fig. 7. Peaks A and C are attributed to the reduction of $PbO + PbO{\cdot}PbSO_4$ (i.e., Pb^{2+}) to Pb, and peaks B and D to the reduction of $PbSO_4$ to Pb [14]. Addition of lithium to the Pb–Ca–Sn alloy is probably beneficial to decrease the reduction charges for $PbO + PbO{\cdot}PbSO_4$ (i.e., Pb^{2+}) and $PbSO_4$ to Pb. The peak currents of $PbSO_4$/Pb reaction (peaks B and D) did not vary significantly for anodization time longer than 20 min (Fig. 8A). So, this behavior does not clarify any point for the effect of Li addition to Pb–Ca–Sn alloy.

However, the peak currents (A and C) for Pb^{2+}/Pb reaction increase with the oxidation time. Variation of the anodic charges as functions of anodization time obtained for Pb–Ca–Sn (Fig. 7, curve 1, peak A) and Pb–Ca–Sn–Li (Fig. 7, curve 2, peak C) showed a linear behavior with slopes of 31.32 and 21.15 μC cm^{-2} s^{-1} (Fig. 8B) indicating the growth rate of Pb^{2+} film on Pb–Ca–Sn (curve a) and Pb–Ca–Sn–Li (curve b) alloys, respectively. Therefore, addition of lithium into Pb–Ca–Sn alloy

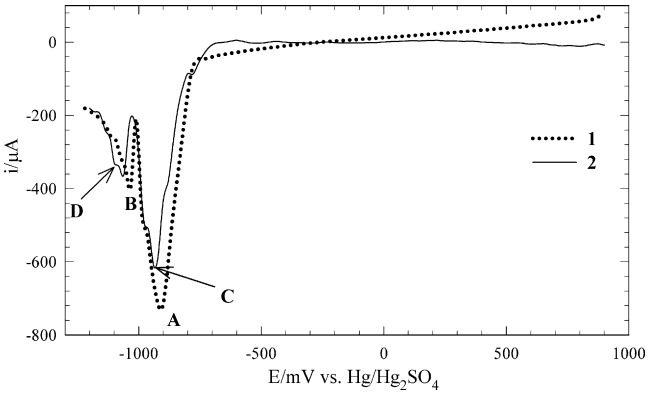

Fig. 7. Linear sweep voltammograms obtained for anodic films formed on (1) Pb–Ca–Sn and (2) Pb–Ca–Sn–Li electrodes after 30 min anodization at +0.900 V in 4.5 M H_2SO_4 at 25 °C and then sweeping the potential to −1.2 V with 1 mV s^{-1} scan rate.

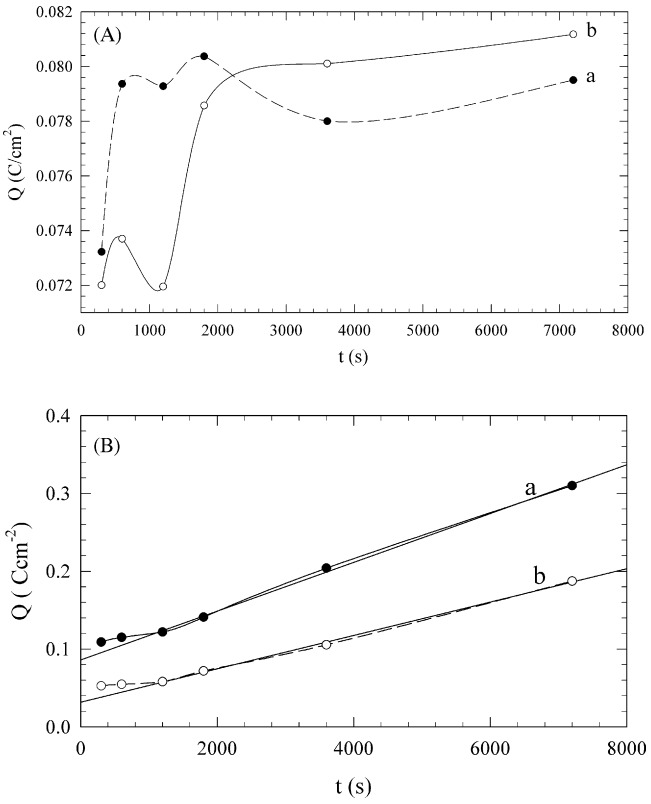

Fig. 8. (A) Variation of reduction charges vs. time of anodization for $PbSO_4$/Pb peak evaluated from linear sweep voltammograms (Fig. 7, peaks B and D) for the anodic films formed on (a) Pb–Ca–Sn and (b) Pb–Ca–Sn–Li electrodes at +0.900 V. (B) Variation of reduction charges as functions of anodization time evaluated from surface area of Pb^{2+}/Pb anodic peaks (Fig. 7, peaks A and C) on (a) Pb–Ca–Sn and (b) Pb–Ca–Sn–Li electrodes, respectively.

can obviously decrease anodic growth of the Pb^{2+} film and increase the corrosion resistance of the alloy.

4. Conclusion

The addition of lithium into Pb–Ca–Sn has led to the formation of Pb–Ca–Sn–Li alloy, decrease the corrosion rate of the alloy by a factor of 2.65 (from 134.2 to 50.3 mpy), and inhibition the growth of the anodic Pb^{2+} film formed at +0.900 V by using Tafel plots. Cyclic polarization measurements revealed no pitting corrosion for the alloy. Variation of the anodic charges as functions of anodization time obtained by LSV showed that the formation rate of Pb^{2+} film on Pb–Ca–Sn–Li alloy has considerably decreased, and confirmed the increase of corrosion resistance of the alloy. These behaviors have been established by the EIS studies in a wide range of dc potentials.

Therefore, addition of Li into Pb–Ca–Sn alloy can obviously improve the corrosion resistance of the alloy and form a new positive grid material, Pb–Ca–Sn–Li, for lead-acid.

Acknowledgement

The authors gratefully acknowledge the University of Isfahan for providing the research facilities.

References

[1] (a) S. Zhong, J. Wang, H.K. Liu, S.X. Dou, M. Skyllas-Kazacos, J. Power Sources 66 (1997) 107–113;
(b) W.H. Boctor, S. Zhong, H.K. Liu, S.X. Dou, J. Power Sources 77 (1999) 56–63.
[2] N. Koura, T. Sakaue, J. Power Sources 69 (1997) 69–74.
[3] J. Yamashita, H. Yufu, Y. Matsumaru, Denki Kagoku 56 (1988) 961.
[4] Z.I. Takehara, J. Power Sources 85 (2000) 29–37.
[5] D. Pavlov, Electrochim. Acta 23 (1978) 845–854.
[6] B. Culpin, A.F. Hollenkamp, D.A. Rand, J. Power Sources 38 (1992) 63–74.
[7] R.F. Nelson, D.M. Wisdom, J. Power Sources 33 (1991) 165–185.
[8] E. Hameenoja, T. Laitinen, G. Sundholm, A. Yli-Pentti, Electrochim. Acta 34 (1989) 233–241.
[9] D. Slavkov, B.S. Haron, B.N. Popov, F. Fleming, J. Power Sources 112 (2002) 199–206.
[10] H.T. Liu, J. Yang, H.H. Liang, J.H. Zhuang, W.F. Zhou, J. Power Sources 93 (2001) 230–233.
[11] (a) D. Pavlov, in: B.D. McNicol, D.A.J. Rand (Eds.), Power Sources for Electrical Vehicles, Elsevier, Amsterdam, 1984;
(b) J.A. Bialacki, N.A. Hampson, F.J. Wilson, J. Appl. Electrochem. 15 (1985) 99–105.
[12] B.K. Mahato, J.L. Strebe, D.F. Wilkinson, K.R. Bullock, J. Electrochem. Soc. 132 (1985) 19–23.
[13] J. Hertz, C. Forniaseri, J.P. Hilger, M. Notin, J. Power Sources 46 (1993) 299–310.
[14] (a) E. Rocca, J. Steimetz, Electrochim. Acta 44 (1999) 4611–4618;
(b) G. Bourguignon, A. Maitre, E. Rocca, J. Steinmetz, L. Torcheux, J. Power Sources 113 (2003) 301–307.
[15] D. Pavlov, B. Monakhov, M. Maja, N. Penazzi, J. Electrochem. Soc. 136 (1989) 27–33.
[16] J.L. Caillerie, L. Albert, J. Power Sources 67 (1997) 279–281.
[17] N. Bui, P. Mattesco, P. Simon, N. Pebere, J. Power Sources 73 (1998) 30–35.
[18] N. Bui, P. Mattesco, P. Simon, J. Steinmetz, E. Rocca, J. Power Sources 67 (1997) 61–67.
[19] (a) E. Barsoukov, J.R. Macdonald (Eds.), Impedance Spectroscopy, Theory, Experiment and Applications, second ed., Wiley-Interscience, New York, 2005;
(b) J. Ross Macdonald, Solid State Ionics 176 (2005) 1961–1969.
[20] (a) R. Jurczakowski, C. Hitz, A. Lasia, J. Electroanal. Chem. 572 (2004) 355–366;
(b) R. Jurczakowski, C. Hitz, A. Lasia, J. Electroanal. Chem. 582 (2005) 85–96;
(c) A. Lasia, A. Rami, J. Electroanal. Chem. 294 (1990) 123–141;
(d) B. Boukamp, Solid State Ionics 18 and 19 (1986) 136–140;
(e) B. Boukamp, Solid State Ionics 20 (1986) 31–44.

[21] J.R. Scully, Corrosion 56 (2000) 199–218.
[22] F. Mansfeld, W.J. Lorenz, in: R. Varma, J.R. Selman (Eds.), Techniques for Characterization of Electrodes and Electrochemical Processes, Wiley, New York, 1991, pp. 581–647.
[23] A. Lasia, in: R.E. White, B.E. Conway, J.O'M. Bockris (Eds.), Modern Aspects of Electrochemistry, vol. 32, Kluwer Academic/Plenum Press, New York, 1999, pp. 143–248.
[24] G. Inzelt, G. Lang, J. Electroanal. Chem. 378 (1994) 39–49.
[25] J. Benavente, J.R. Ramos-Barrado, A. Cabeza, J. Colloid Interface Sci. 180 (1996) 116–121.
[26] T.M. Nahir, E.F. Bowden, Electrochim. Acta 39 (1994) 2347–2352.
[27] R.P. Janek, W.R. Fawcett, A. Ulman, J. Phys. Chem. B 101 (1997) 8550–8558.
[28] L.V. Protsailo, W.R. Fawcett, Electrochim. Acta 45 (2000) 3497–3505.
[29] M. Metikoš-Huković, R. Babić, S. Brinić, J. Power Sources 157 (2006) 563–570.
[30] S. Brinić, M. Metikoš-Huković, R. Babic, J. Power Sources 55 (1) (1995) 19–24.
[31] R. Karimi Shervedani, S.A. Mozaffari, Anal. Chim. Acta 562 (2) (2006) 223–228.